# Optimizing Temperature and Flow Fields of 4H-SiC Epitaxial Growth by Integrating CFD Simulation with Multi-objective Particle Swarm Optimization

Tian, Jing; Tang, Zhuorui; Tang, Hongyu; Fan, Jiajie; Zhng, Guoqi

**DOI**
10.1109/ICEPT59018.2023.10492175

**Publication date**
2023

**Document Version**
Final published version

**Published in**
International Conference on (ICEPT) Electronic Packaging Technology

**Citation (APA)**
Tian, J., Tang, Z., Tang, H., Fan, J., & Zhng, G. (2023). Optimizing Temperature and Flow Fields of 4H-SiC Epitaxial Growth by Integrating CFD Simulation with Multi-objective Particle Swarm Optimization. In *International Conference on (ICEPT) Electronic Packaging Technology* IEEE. https://doi.org/10.1109/ICEPT59018.2023.10492175

# Optimizing Temperature and Flow Fields of 4H-SiC Epitaxial Growth by Integrating CFD Simulation with Multi-objective Particle Swarm Optimization

Jing Tian
Academy for Engineering & Technology, Fudan University, Shanghai 200433, China

Zhuorui Tang
Academy for Engineering & Technology, Fudan University, Shanghai 200433, China

Hongyu Tang
Academy for Engineering & Technology, Fudan University, Shanghai 200433, China

Jiajie Fan*
Academy for Engineering & Technology, Fudan University, Shanghai 200433, China
Research Institute of Fudan University in Ningbo, Ningbo 315336, China
jiajie_fan@fudan.edu.cn

Guoqi Zhng
EEMCS Faculty, Delft University of Technology, Delft 2628CD, the Netherlands

2023 24th International Conference on Electronic Packaging Technology (ICEPT) | 979-8-3503-3881-2/23/$31.00 ©2023 IEEE | DOI: 10.1109/ICEPT59018.2023.10492175

***Abstract*—The silicon carbide (SiC) epitaxial growth process is crucial in chip manufacturing. The distribution of the flow and temperature fields in the reactor chamber influences the epitaxial layer uniformity. Therefore, this study optimizes the distribution of the flow and temperature fields inside the reactor to enhance the quality of the epitaxial layer. COMSOL Multiphysics is used to model the horizontal chemical vapor deposition (CVD) reactor chamber, and the flow and temperature fields inside the reactor chamber are analyzed. Factors influencing the uniformity of flow field distribution include the reactant gas distribution and the gas-inlet tunnel's diameter and position. The flow field uniformity is represented by the relative standard deviation of the velocity. Parameters impacting the temperature field uniformity include the position and pitch of the heating coil and the graphite column width. The heating efficiency of the substrate and temperature uniformity are expressed by the average temperature and standard deviation of the temperature, respectively. Support vector machine (SVM) is used to establish the relationship between design variables and the objective function, and the multi-objective particle swarm optimization (MOPSO) algorithm is used to optimize the reactor. The proposed approach improves the uniformity of the flow and temperature fields and the heating efficiency of the substrate.**

***Keywords—Silicon carbide, Epitaxial growth, Multi-objective optimization, SVM, MOPSO***

## I. *Introduction*

Silicon carbide (SiC), a third-generation semiconductor material, exhibits numerous advantages compared to first and second-generation semiconductor materials and possesses a wide gap band, high critical breakdown electric field, high thermal conductivity, and high electron saturation drift rate [1-3]. Therefore, SiC devices hold immense potential for various applications in power electronics, aerospace, wireless communication, and other fields. The SiC epitaxial layer with fewer defects and more uniform thickness can produce a better performance of SiC devices. Therefore, optimizing SiC epitaxial growth process is a significant area of research.

The flow field and substrate temperature distribution significantly affect the thickness uniformity and growth of the SiC epitaxial layer, respectively. An uneven flow field deteriorates the uniformity of the SiC epitaxial layer [4, 5]. Substantial temperature variations on the substrate can cause uneven doping, thickness, and interfacial state [6, 7]. Therefore, improving the uniformity of flow and temperature fields is crucial. Flow and temperature fields are vital control factors for crystal preparation in the SiC epitaxy process, impacting crystal growth uniformity. Consideration of their influence and implementation of corresponding control measures are essential for optimizing the SiC epitaxy process, ensuring crystal growth uniformity and quality.

Simulating the flow and temperature fields helps determine suitable thermodynamic experiments and process parameters, reducing the complexity, time, and cost of the experiment and improving the experiment's feasibility [8]. Optimizing simulation results can identify potential code optimizations and aid in making informed market decisions. Tang *et al.* [9] enhanced substrate temperature uniformity by incorporating a graphite column beneath the reactor base. However, the relationship between the graphite column and the temperature field uniformity in depth was not explored. Chen Tao et al. improved the flow field uniformity in the reaction chamber by altering gas flow velocity distributions [4]. However, the study was limited to a few specific velocity distributions. Although they optimized the flow field uniformity to a certain extent, their approach lacked precision.

This study optimizes the temperature field of the SiC epitaxy reactor and the flow field in the reaction chamber. The substrate flow field uniformity, heating efficiency, and temperature uniformity are assessed using the relative standard deviation of the velocity, average temperature, and standard deviation of the temperature, respectively. The geometric model of the SiC epitaxial reactor is established using COMSOL Multiphysics. Subsequently, the flow and temperature fields are simulated, and the results are fitted using support vector regression (SVR) and optimized using

multi-objective particle swarm optimization (MOPSO) to determine the optimal solution for the objective function.

## II. *Computational Modeling*

This study constructs a horizontal chemical vapor deposition (CVD) reactor model (Fig. 1(a)), with the reactor's upper and lower bases made of dense graphite material and 11 turns of rectangular coils wound around them. After the alternating current is passed through the coil, eddy currents are induced within the graphite base due to electromagnetic induction, generating substantial heat and elevating the internal temperature. Introducing a graphite pillar beneath the graphite pedestal surges heat conduction in the reactor, resulting in higher substrate temperature and improved temperature uniformity (Fig. 1(b)). The grid division of the reactor (Fig. 3) illustrates the importance of refining meshes of graphite and substrate areas for studying temperature distribution.

The reaction chamber is at the center of the reactor (Fig. 3), comprising 26 gas-inlet tunnels are set for the reactor divided into three groups: 16 in the middle and five on the left and right sides (Fig. 4). The three groups of the gas-inlet tunnel are color-coded to facilitate observation. The grid division of the reaction chamber (Fig. 3) is re-divided during the flow field simulation. The free meshing technique is employed due to the relatively simple structure of this section.

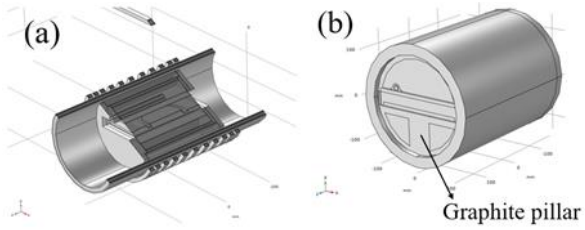


Fig. 1. (a) Section view of reactor structure. (b) Schematic diagram of graphite column.

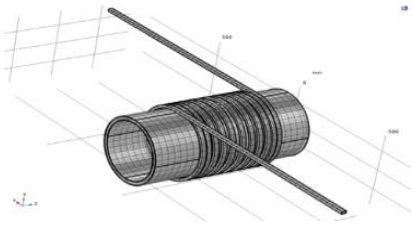

Fig. 2. FEM mesh of 3D model reactor.

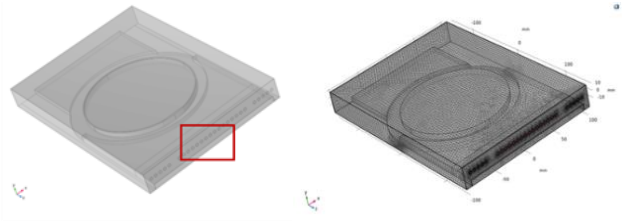

Fig. 3. Reaction chamber structure diagram and meshing.

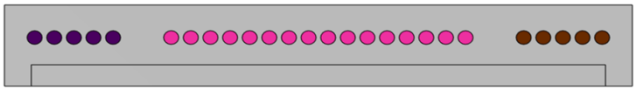

Fig. 4. Gas-inlet tunnel diagram.

## III. Process Optimization of the Flow and Temperature Fields

### A. Support Vector Machine Regression

Support vector machine (SVM) is a supervised learning model for classification and regression analysis. The fundamental principle involves identifying the "optimal interval hyperplane" to separate samples of different categories. The term "optimal interval hyperplane" refers to the hyperplane that maximizes the sum of distances from the sample closest points of each category to the hyperplane. An SVM is a binary classifier that can be extended to multi-classification problems by training it iteratively. SVM classifiers have been widely used in supervised learning applications, including text classification, image classification, bioinformatics, and speech recognition.

When SVM is used to solve regression problems, its objective function form can be derived from the following steps [10, 11].

For a given dataset

$$D = \{(x_1, y_1), (x_2, y_2) \ldots, (x_m, y_m)\}, y_i \in \mathbb{R} \quad (1)$$

a hyperplane can be determined as follows

$$f(x) = w^T x + b \quad (2)$$

to minimize the discrepancy between the model's predicted value $f(x_i)$ for sample $x_i$ and its corresponding label $y_i$. SVR can tolerate $\epsilon$ deviation between $f(x_i)$ and $y_i$. When the deviation is less than $\epsilon$, the loss is 0; when the deviation exceeds $\epsilon$, the loss is non-zero. An $\epsilon$-insensitive loss function (3) is introduced to represent the loss of each sample in the SVR problem.

$$l_\varepsilon(f(x_i) - y_i) = \begin{cases} 0 & |f(x_i) - y_i| \le \varepsilon \\ |f(x_i) - y_i| - \varepsilon, & |f(x_i) - y_i| > \varepsilon \end{cases} \quad (3)$$

The samples whose deviation exceeds $\epsilon$ are called support vectors, and their error is $|f(x_i) - y_i| - \varepsilon$ .

Slack variables are introduced in SVR

$$\xi_i + \hat{\xi}_i = l_\varepsilon(f(x_i) - y_i) \quad (4)$$

at this stage, the objective function can be rewritten as

$$\begin{aligned} &\min_{w,b,\xi_i,\hat{\xi}} \frac{1}{2} w^T w + C\Sigma_{i=1}^{m}(\xi_i + \hat{\xi}) \\ &s.t. f(x_i) - y_i \le \varepsilon + \xi_i \\ &y_i - f(x_i) \le \varepsilon + \hat{\xi}_i \\ &\xi_i \ge 0, \\ &\hat{\xi}_i \ge 0 \end{aligned} \quad (5)$$

The Lagrange formula for SVR problem is as follows

$$L(w,b,\alpha,\hat{\alpha},\hat{\xi}_i,\xi_i,\lambda,\hat{\lambda}) =$$
$$\frac{1}{2}w^T w + C\sum_{i=1}^{m}(\xi_i+\hat{\xi}_i) - \sum_{i=1}^{m}\lambda_i\xi_i - \sum_{i=1}^{m}\hat{\lambda}_i\hat{\xi}_i +$$
$$\sum_{i=1}^{m}\alpha_i(f(x_i)-y_i-\varepsilon-\xi_i) + \sum_{i=1}^{m}\hat{\alpha}_i(y_i-f(x_i)-\varepsilon-\hat{\xi}_i) \tag{6}$$

The gradients to $w,b,\xi_i,\hat{\xi}_i$ are 0, and we obtain

$$w = \sum_{i=1}^{m}(\hat{\alpha}_i-\alpha_i)x_i \tag{7}$$

Then the solution of SVR is

$$f(x) = \sum_{i=1}^{m}(\hat{\alpha}_i-\alpha_i)x_i^T x + b \tag{8}$$

Consider the following feature map form：

$$w = \sum_{i=1}^{m}(\hat{\alpha}_i-\alpha_i)\phi(x) \tag{9}$$

Then the final form of SVR is

$$f(x) = \sum_{i=1}^{m}(\hat{\alpha}_i-\alpha_i)\kappa(x_i^T x) + b \tag{10}$$

where $\kappa(x_i^T x) = \phi(x_i)^T\phi(x_j)$ is the kernel function.

### *B. Multi-objective Particle Swarm Optimization*

Particle swarm optimization (PSO) is an optimization algorithm based on swarm intelligence, simulating the foraging behavior of birds to determine the optimal solution foraging. This algorithm suits global optimization across various solution spaces [12, 13].

In the PSO algorithm, solutions are presented as positions of particles within the solution space. Each particle has its own velocity and position, which vary randomly over time when the particle compares the distance between the current position and the best position. In addition, the particle also compares the best position in the group.

During each position update, the fitness value is calculated, and the individual and group extrema Pbest and Gbest, respectively, are updated by comparing the fitness values of the new particle with the individual and group extrema.

During each iteration, the particle updates its velocity and position through the individual and group extrema using (11):

$$\begin{aligned} V_{id}^{k+1} &= \omega V_{id}^{k} + c_1 r_1 (P_{id}^{k} - X_{id}^{k}) + c_2 \\ X_{id}^{k+1} &= X_{id}^{k} + V_{id}^{k+1} \end{aligned} \tag{11}$$

The PSO offers the advantage of determining optimal solutions in a vast search space while mitigating the risk of getting trapped in local optima. This algorithm has applications in diverse fields, such as machine learning, artificial intelligence, economics, biology, and physics.

This study uses the SVR to construct a functional relationship between the objective function and the optimization variables. Moreover, the PSO algorithm or MOPSO algorithm is used to find the optimal solution of the objective function. The optimization flow chart is shown in Fig. 5.

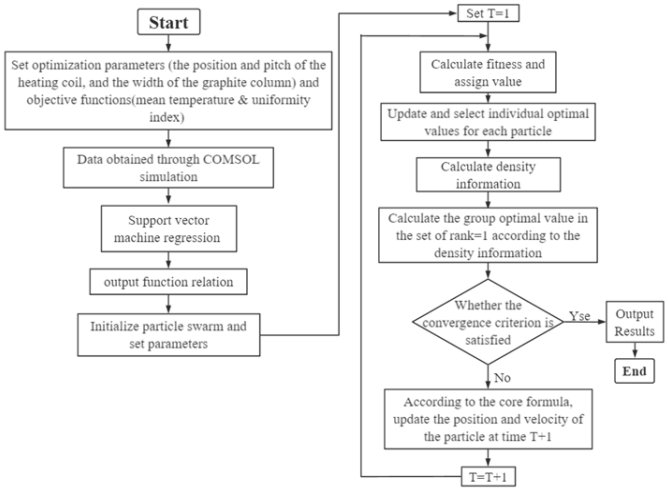


Fig. 5. Multi-objective Particle Swarm Optimization Flowchart.

### *C. Orthogonal Experimental Design*

Orthogonal experimental design is an approach to investigate multi-factor and multi-level studies, which selects representative points from the comprehensive test according to the orthogonality. These representative points possess characteristics of uniform dispersion, order, and comparability. Orthogonal experimental design is predominantly employed in a fractional factorial design and serves as an efficient, rapid, and economical experimental design method. The orthogonal experimental design technique utilizes existing tables to arrange experiments and conduct data analysis.

In the flow field simulation, the spacing and diameter of the inlet holes exhibit a dependent relationship, rendering the use of orthogonal experiments impractical. However, the three parameters in the temperature field simulation are independent of each other, allowing for the adoption of an orthogonal experiment.

### *D. Flow Field Simulation and Optimization*

Due to the fact that only a small portion of the reactive gas enters the reaction chamber, and most of it is hydrogen gas as the carrier gas, only hydrogen gas is considered in the flow field simulation, without considering other reactive gases. Therefore, the proportion of each part of the gas does not need to be considered during simulation optimization.

The air inlets of the epitaxial furnace reaction chamber are arranged in three groups, with a distribution ratio in each group is 6:16:6. These air inlets are symmetrically positioned on the left and right sides, resulting in a symmetrical distribution of airflow within the reaction chamber. When the total gas flow is constant, the gas flow ratio among the inlet groups significantly impacts the flow field distribution in the reaction chamber, making it an important parameter. In addition, the position of each air inlet affects the flow field distribution at the inlet, influencing the overall flow field distribution of the reaction chamber. Moreover, the diameter of the gas inlet can alter the gas velocity at the inlet, affecting the flow field in the reaction chamber. Therefore, the optimization problem has three parameters: gas distribution ratio, gas inlet position, and gas inlet diameter, and their range settings are illustrated in Table 1.

The uniformity of the flow field can be represented by the relative standard deviation of the velocity (12) [14]:

$$C_v = \frac{\sigma}{\bar{v}} \times 100\% \tag{12}$$

where

$$\sigma = \sqrt{\frac{1}{n-1}\sum_{i=1}^{n}\left(v_i - \bar{v}\right)^2} \tag{13}$$

and $\bar{v}$ is the average speed.

TABLE I. FLOW FIELD OPTIMIZATION PARAMETERS

| Design variables | Ranges |
|---|---|
| Gas flow in the middle inlet (vl) | 70-110 (l/min) |
| Diameter of the gas-inlet tunnel (r) | 1-3.5 (mm) |
| Inlet spacing (d) | 2.51-7.51 (mm) |

### E. Temperature Field Simulation Optimization

The addition of a graphite column alters part of the heat transfer mode from radiation to conduction, improving the heat transfer efficiency. Modifying the width of the graphite column influences the heating efficiency and temperature uniformity of the substrate. Therefore, replacing a single graphite column with a graphite grid composed of multiple graphite columns might further enhance the substrate's heating efficiency and temperature uniformity. The epitaxial furnace employs electromagnetic induction to heat the reaction chamber, and the magnetic field distribution of the epitaxial furnace affects its heating efficiency and temperature uniformity. Modifying the overall position of the coil or adjusting the pitch of each turn coil changes the distribution of the magnetic field. Therefore, optimizing the epitaxial furnace structure requires consideration of changing the coil turns and pitch. The optimization problem encompasses three variables: coil position (*dl*), coil pitch (*dz*), and graphite column width (*wid*). The range settings of these parameters are shown in Table 2. The pitch parameter refers to uniformly changing the pitch of each coil turn based on the original.

TABLE II. TEMPERATURE FIELD OPTIMIZATION PARAMETERS

| Design variables | Ranges |
|---|---|
| Coil position (*dl*) | -10-28 (mm) |
| Pitch parameter (*dz*) | -2-3 (mm) |
| Graphite column width (*wid*) | 20-45 (mm) |

## IV. RESULT AND DISCUSSION

### A. Flow Fields

The flow field results (Figs. 8 and 9) indicate a strong agreement between the fitted data and actual values with minimal errors. Data normalization is performed to ensure the prediction accuracy of the SVR model to fit the data and prevent significant value gaps of each independent variable from affecting the results. The normalization function is as follows:

$$y = \frac{(y_{\max} - y_{\min})(x - x_{\min})}{x_{\max} - x_{\min}} + y_{\min} \tag{14}$$

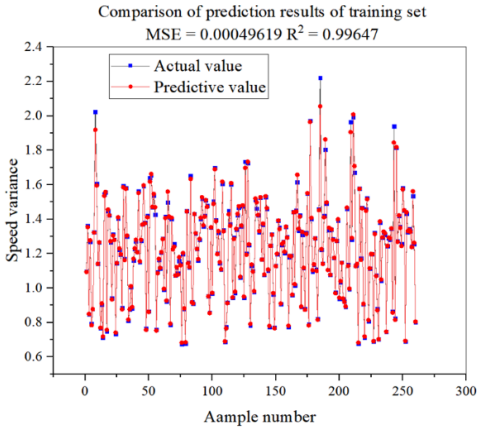


Fig. 6. The training set fitting results of the flow field.

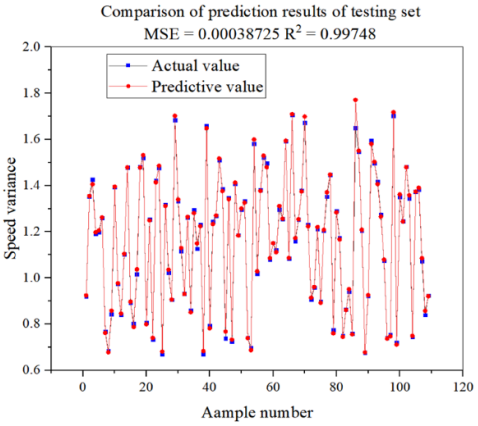


Fig. 7. The testing set fitting results of the flow field.

The objective function comprises three independent variables. Therefore, one of the parameters needs to be fixed, allowing an image of the objective function to be created with the other two parameters, as shown in Fig. 10, which illustrates the approximate location of the optimal point of the objective function.

The PSO algorithm is used to determine the minimum value of the objective function, obtaining the following parameters of the most stable flow field in the reaction chamber:

$$\begin{aligned} vl &= 91.23\ l/min \\ d &= 7.20\ mm \\ r &= 3.55\ mm \end{aligned} \tag{15}$$

The convergence process is shown in Fig. 11, illustrating the iterative progress toward convergence. The flow field is simulated again at the optimum point, and the obtained flow field results are shown in Fig. 12.

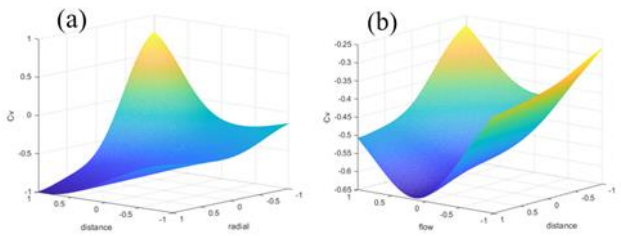

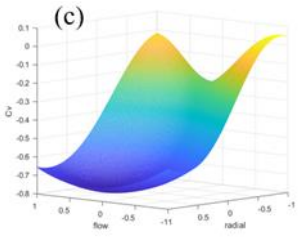


Fig. 8. Functional graph of objective function and parameters (normalized). This simulation has fixed (a) gas flow in the middle inlet, (b) diameter of the gas-inlet tunnel, and (c) inlet spacing.

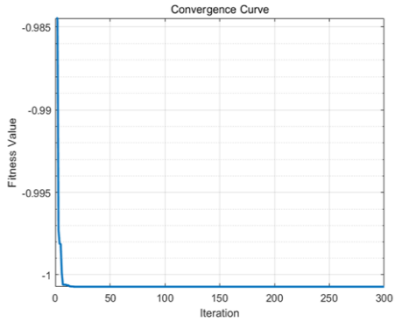


Fig. 9. Convergence process diagram.

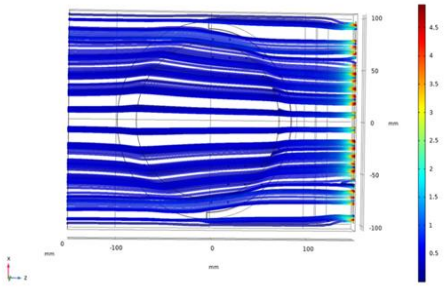

Fig. 10. Optimized flow field.

## B. *Temperature Field*

The optimization problem of the temperature field involves two objective functions: the average temperature and temperature standard deviation. Separate SVR models are utilized to fit the two objective functions to address each objective function (Figs. 12 and 13). The small fitting error indicates a close approximation between the fitted and true functions.

The function images of two objective functions and independent variables of the temperature field are generated using the same methodology in Fig. 8.

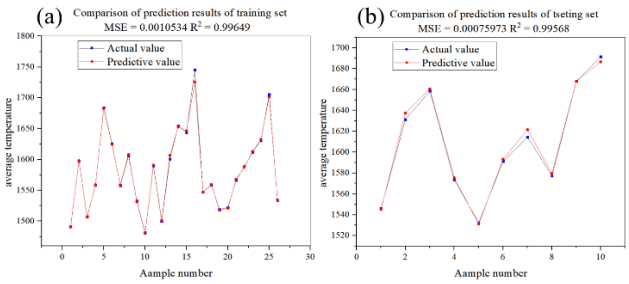


Fig. 11. Average temperature fitting results of (a) the training set and (b) the testing set.

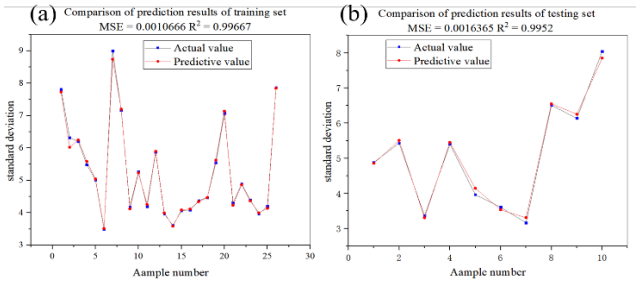


Fig. 12. Temperature standard deviation fitting results of (a) the training set and (b) the testing set.

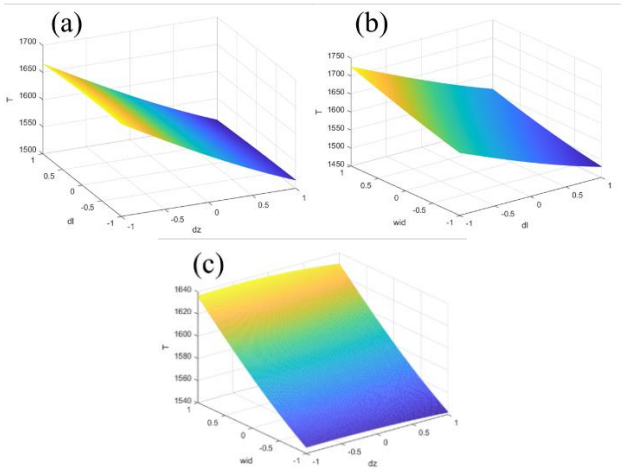


Fig. 13. Functional graph of objective function and normalized parameters with fixed (a) wid (b) dz and (c) dl.

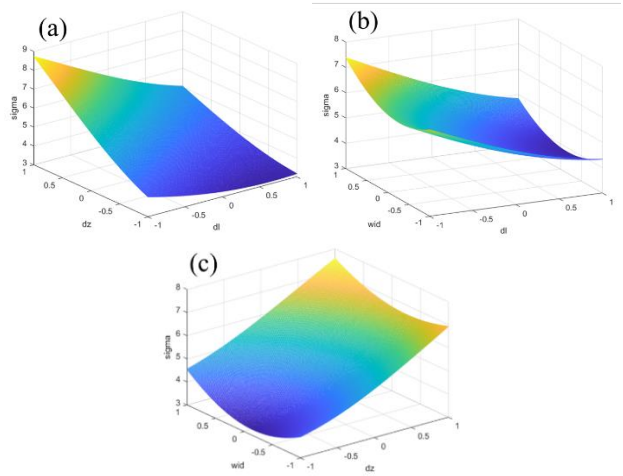


Fig. 14. Functional graph of objective function and normalized parameters with fixed (a) wid (b) dz (c) dl.

The Pareto front of the two objective functions (average temperature and temperature standard deviation) represents the optimal advantage (Fig. 15). An optimal point in the Pareto front is a point where no objective function can be improved without worsening at least another objective function. In other words, by moving over the points shown in Fig. 15, the condition of one objective function gets better, while the condition of the other objective function becomes worse [15]. Among them, the four points indicated in the figure are the four best points selected in this study. The substrate temperature distribution at the four optimum points and the

independent variables are shown in Fig. 16 and Table 3, respectively.

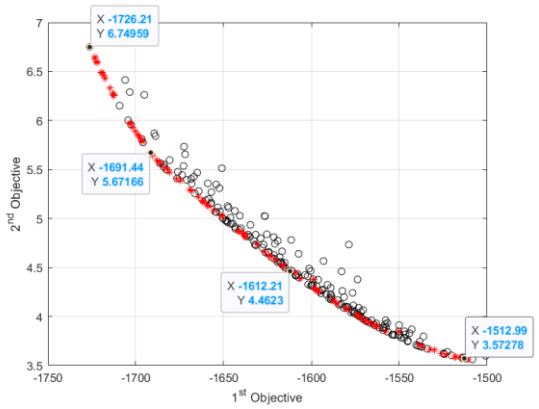


Fig. 15. Pareto front of the two objectives: average temperature and temperature standard deviation.

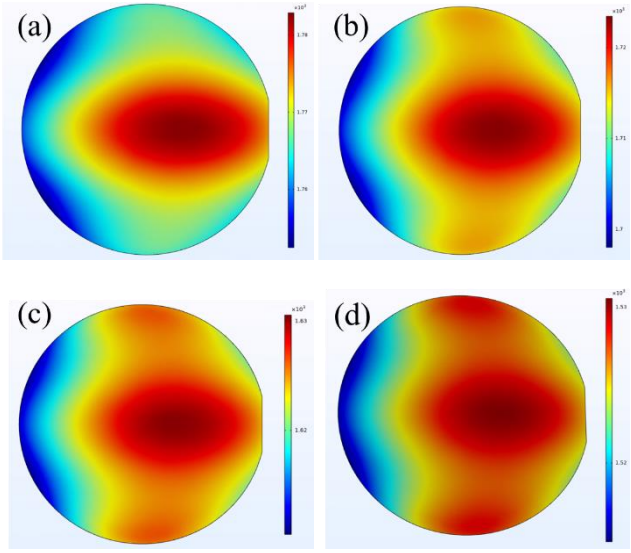


Fig. 16. Temperature distribution of substrate at optimum points (a) ,(b), (c) and (d).

TABLE III. THE ARGUMENT AT THE OPTIMAL SOLUTION

| | dl | dz | **wid** |
|---|---|---|---|
| a | -2.00 mm | 3.3 mm | 45.00 mm |
| b | -2.00 mm | 3.3 mm | 37.23 mm |
| c | -0.03 mm | 3.3 mm | 34.67 mm |
| d | 3.00 mm | 3.3 mm | 32.15 mm |

The objective function values of the optimal points a to d obtained by SVM and optimization method are further analyzed using the COMSOL simulation environment. The results (Table 4) indicate a close agreement between the calculation results of the two methods, with a maximum calculation error of 4.80%.

TABLE IV. RE-EVALUATION OF THE OBTAINED OPTIMAL PARETO FRONT USING COMSOL.

| Points | Average temperature (℃) | | Temperature standard deviation | | |
|---|---|---|---|---|---|
| | SVR | COMSOL | Error (%) | SVR | COMSOL | Error (%) |
| a | 1726.2 | 1770.2 | 2.49 | 6.7496 | 6.9430 | 2.79 |
| b | 1691.4 | 1714.1 | 1.32 | 5.6717 | 5.4760 | 3.45 |
| c | 1612.2 | 1623.9 | 0.72 | 4.4623 | 4.3125 | 3.36 |
| d | 1513.0 | 1525.7 | 0.83 | 3.5728 | 3.4013 | 4.80 |

## V. CONCLUSIONS

SiC epitaxy is a crucial process in semiconductor device manufacturing. However, optimizing the process flow and temperature fields is challenging. This study addressed this issue by employing the MOPSO algorithm to optimize the flow and temperature fields of SiC epitaxial. SVR was used to establish the functional relationship between the objective function and the optimization variables, enabling optimization of the flow and temperature fields. The experimental results demonstrated that the MOPSO algorithm improved the performance of SiC epitaxial flow and temperature fields. The proposed approach offered a more optimized and feasible solution for the SiC epitaxial growth process by considering multiple objective functions. Therefore, the manufacturing quality and reliability of semiconductor devices could be significantly improved.

## ACKNOWLEDGMENTS

This work was partially supported by National Natural Science Foundation of China (52275559), Shanghai Pujiang Program (2021PJD002), Taiyuan Science and Technology Development Funds (Jie Bang Gua Shuai Program) and Shanghai Science and Technology Development Funds (19DZ2253400, 20501110700).

## REFERENCES

[1] L. Spaziani, L. Lu, and Ieee, "Silicon, GaN and SiC: There's Room for All An application space overview of device considerations," in *30th IEEE International Symposium on Power Semiconductor Devices and ICs (ISPSD)*, Chicago, IL, May 13-17 2018,

[2] N. Yingxi, " The 4H-SiC Thick Homoepitaxial Key Technologies Research and Device Verification ", Xidian University, 2020.

[3] H. Yanjing, "The Study on the Design and Key Process of Advanced 4H-SiC VDMOSFETs," Xidian University, 2018.

[4] C. Tao, L. Mingda, and L. Yang, "Simulation of Flow Field in CVD Epitaxy Base on Laminar Model," *Research & Progress of SSE* vol. 37, no. 06, pp. 438-442, 2017, doi: 10.19623/j.cnki.rpsse.2017.06.014.

[5] M. Bai, S. Wen, J. Zhao, Y. Du, F. Xie, and H. Liu, "Effect of Carrier Gas Flow Field on Chemical Vapor Deposition of 2D MoS2 Crystal," *Coatings,* vol. 11, no. 5, 2021, doi: 10.3390/coatings11050547.

[6] Y. Xinqiang, "Study of Material Characterization and Temperature Modeling of Silicon Carbide Epilayer," Xidian University, 2007.

[7] Y. Niu *et al.*, "The influence of temperature on the silicon droplet evolution in the homoepitaxial growth of 4H-SiC," *Journal of Crystal Growth,* vol. 504, pp. 37-40, 2018, doi: 10.1016/j.jcrysgro.2018.09.022.

[8] T. Zhuorui, W. Huiyong, K. Qianyin, Z. Nan, and H. Jiyu, "Design and Simulation for Induction Heating Reactor of Silicon Carbide Epitaxial Growth," *Mechanical & Electrical Engineering Technology* vol. 51, no. 12, pp. 248-252, 2022.

[9] Z. Tang *et al.*, "Temperature Field Simulation and optimization for Horizontal 6-inch 4H-SiC Epitaxial CVD Reactor by Induction

Heating," presented at the 2023 24th International Conference on Thermal, Mechanical and Multi-Physics Simulation and Experiments in Microelectronics and Microsystems (EuroSimE), 2023.

[10] A. J. Smola and B. Schölkopf, "A tutorial on support vector regression," *Statistics and Computing,* vol. 14, no. 3, 2004.

[11] S. Herceg, Ž. Ujević Andrijić, and N. Bolf, "Development of soft sensors for isomerization process based on support vector machine regression and dynamic polynomial models," *Chemical Engineering Research and Design,* vol. 149, pp. 95-103, 2019, doi: 10.1016/j.cherd.2019.06.034.

[12] G. Wang, G. Zhao, H. Li, and Y. Guan, "Multi-objective optimization design of the heating/cooling channels of the steam-heating rapid thermal response mold using particle swarm optimization," *International Journal of Thermal Sciences,* vol. 50, no. 5, pp. 790-802, 2011, doi: 10.1016/j.ijthermalsci.2011.01.005.

[13] Z. Liu, C. Zhu, P. Zhu, and W. Chen, "Reliability-based design optimization of composite battery box based on modified particle swarm optimization algorithm," *Composite Structures,* vol. 204, pp. 239-255, 2018, doi: 10.1016/j.compstruct.2018.07.053.

[14] S. J. Wang, P. Zhu, G. Zhang, Q. Zhang, Z. Y. Wang, and L. Zhao, "Numerical simulation research of flow field in ammonia-based wet flue gas desulfurization tower," *Journal of the Energy Institute,* vol. 88, no. 3, pp. 284-291, 2015, doi: 10.1016/j.joei.2014.09.002.

[15] M. Darvish Damavandi, M. Forouzanmehr, and H. Safikhani, "Modeling and Pareto based multi-objective optimization of wavy fin-and-elliptical tube heat exchangers using CFD and NSGA-II algorithm," *Applied Thermal Engineering,* vol. 111, pp. 325-339, 2017, doi: 10.1016/j.applthermaleng.2016.09.120.